TU Delft

Delft University of Technology

Document Version
Final published version

Licence
CC BY

Citation (APA)
Sulollari, E., & Meijers, P. C. (2026). Identification of strain-induced effective magnetisation in the presence of pile displacement. In *Proceedings of the 12th European Workshop on Structural Health Monitoring (EWSHM 2026): July 7-10, 2026 in Toulouse, France* Article 1431 (e-Journal of Nondestructive Testing; Vol. 2026, No. 08). NDT.net. https://doi.org/10.58286/33798

Important note
To cite this publication, please use the final published version (if applicable).
Please check the document version above.

Copyright
In case the licence states “Dutch Copyright Act (Article 25fa)”, this publication was made available Green Open Access via the TU Delft Institutional Repository pursuant to Dutch Copyright Act (Article 25fa, the Taverne amendment). This provision does not affect copyright ownership.
Unless copyright is transferred by contract or statute, it remains with the copyright holder.

Sharing and reuse
Other than for strictly personal use, it is not permitted to download, forward or distribute the text or part of it, without the consent of the author(s) and/or copyright holder(s), unless the work is under an open content license such as Creative Commons.

Takedown policy
Please contact us and provide details if you believe this document breaches copyrights.
We will remove access to the work immediately and investigate your claim.

This work is downloaded from Delft University of Technology.

More info about this article: https://www.ndt.net/?id=33798

Identification of strain-induced effective magnetisation in the presence of pile displacement

Enxhi SULOLLARI[1], Peter C. MEIJERS[1]
[1]Delft University of Technology, Delft, the Netherlands,
e.sulollari@tudelft.nl, p.c.meijers@tudelft.nl

Abstract The demand for renewable energy has grown over the past decade and is projected to accelerate further. This rapid growth has led to an increase in offshore wind deployment and to the installation of increasingly larger steel monopiles to accommodate larger turbines. Monitoring of the driving process using conventional contact-based sensors, such as strain gauges and accelerometers, is often not feasible offshore due to harsh installation conditions and the risk of sensor damage. To address this challenge, a novel non-contact sensor system has been developed that uses magnetomechanical effects to infer strain and an optical sensor to measure velocity. Recent full-scale hammer tests have shown that this system can successfully capture strain and velocity during impact piling, allowing for comparison with the contact-based Pile Driving Analyzer, which is the industry standard. However, accurate interpretation of magnetic field signals requires understanding the influence of various magnetic disturbances. This work investigates the interference in magnetic field measurements resulting from pile displacement during hammer impacts. An effective magnetic dipole model is considered to decouple the signal component arising from the pile's displacement from the magnetic changes caused by impact-induced stress. This is achieved by combining theoretical calculations and experimental measurements. By examining how the interference influences the magnetic signal measurements, this study enhances measurement reliability and advances non-contact monitoring technologies for offshore monopile installations.

Keywords: non-contact monitoring; magnetomechanical response; impact pile driving

Introduction

The strive for cleaner energy sources is one of the most demanding problems the world faces today. The role of offshore wind in the energy transition remains crucial in Europe's power system. In 2025, wind supplied 19% of the EU-27's total electricity consumption. Looking ahead, Europe is expected to install an average of 30 GW of new wind capacity per year between 2026 and 2030 [1]. A significant portion of this growth will be driven by offshore developments, which face increasingly complex challenges as they move into harsher environments. As the capacity and size of offshore wind turbines increase, and they are placed in deeper water, their foundation piles, typically steel monopiles, also become larger. This results in additional steel requirement to account for fatigue damage during installation [2], as the fatigue life consumption caused by impact pile driving is not well understood.

To mitigate these uncertainties and optimise steel use, it is important to measure the strain and acceleration of the monopile during installation. Conventional monitoring of steel structures under dynamic loading typically relies on these sensors to be in physical contact with the structure [3, 4]. However, the attachment and detachment of such instrumentation can be cumbersome and, in many offshore scenarios, practically unfeasible [5]. Furthermore,

This work is licensed under CCBY 4.0

Media and Publishing Partner NDT.net
https://doi.org/10.58286/33798

these sensors are prone to damage when subjected to high stress levels during, for example, impact pile driving. Non-contact sensors offer a robust alternative as they do not require physical attachment, making the deployment of the sensor more time and cost-efficient. Recently, a non-contact strain measurement system was proposed and validated for steel monopile installations, relying on the change on the magnetic stray field of the structure to infer the strains through the magnetomechanical effect [6]. The in-situ measurement campaign conducted during the monopile installation was largely successful in demonstrating the practical feasibility of using non-contact magnetic stray field measurements. Magnetic signals showed a very good correlation with actual axial strain recorded by Pile Driving Analysers (PDAs).

The measurement campaign revealed also several challenges regarding measurement consistency particularly across different test orientations. Multiple sources of interference were identified as primary drivers of these inconsistencies [7]. External magnetic fields from nearby ferromagnetic objects, such as the pre-installed outer pile and the hammer-sleeve assembly, distorted the measurements as their distance to the sensor changed during penetration. Additionally, the gradual rotation of the hammer-sleeve assembly relative to the pile affected the comparisons between non-consecutive impacts, while cap pressure within the hammer introduced low-frequency oscillations in nearby sensors. Finally, the ground-based sensors faced inconsistencies due to the relative motion between the stationary sensor and the penetrating pile. As the pile was driven into the soil, its axial position relative to the ground-based magnetometers changed, influenced the magnetic field measurements. This work investigates the interference resulting from pile displacement during hammer impacts. A magnetic dipole model is employed to decouple the signal component arising from the pile's displacement from the magnetic changes induced by hammer impacts. Isolating these effects, a comparison is made between the total measured magnetic field and the extracted stress-induced signal. This differentiation allows for a more precise characterization of the stress-induced magnetisation.

1. Magnetic dipole model

1.1 Static State Initialization

In this section, the theoretical framework used to isolate the change in magnetic signal due to the pile displacement is detailed. The monopile is modeled as an equivalent magnetic dipole $\mathbf{m}$ aligned with the vertical z-axis such that

$$\mathbf{m}(t) = (0, 0, m_z(t)), \tag{1}$$

where $m_z(t)$ accounts for time variations in magnetisation. The magnetic sensor is positioned at a fixed radial distance d from the pile axis at

$$\mathbf{r}_s = (0, d, 0). \tag{2}$$

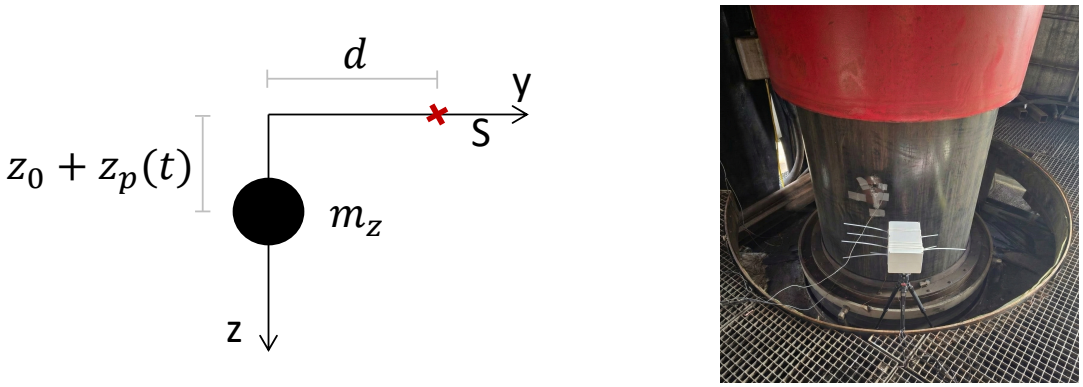
Due to the axisymmetry of the pile geometry, the model considers only the $y - z$ plane as illustrated in the magnetic dipole model in Fig. 1(a), where S denotes the sensor location. The position of the dipole along the monopile is defined as

$$\mathbf{r}_d(t) = (0, 0, z_0 + z_p(t)), \tag{3}$$

where z_0 is the dipole position relative to the sensor before impact, and $z_p(t)$ is the displacement of the pile during impact. This displacement is derived by integrating the measured

This work is licensed under CCBY 4.0

Media and Publishing Partner NDTnet



(a) (b)

Fig. 1. *(a) Magnetic dipole model showing the position of the dipole relative to the sensor; (b) Experimental setup showing the pile and the sensor box looking towards the pile along the y-axis.*

acceleration data using the PDA. The variables $m_z(t)$ and z_0 represent the unknowns to be determined via the measured magnetic field components $B_{y,\text{meas}}$ and $B_{z,\text{meas}}$. These components represent the radial and axial directions, respectively, and are recorded by a bi-axial magnetometer (type: HMC1022). As shown in the experimental setup Fig. 1(b), the sensor is housed in a white box and mounted on a non-magnetic tripod at a distance of $d = 23$ cm from the pile surface. In parallel to the contactless sensor, the hammer-induced strains and acceleration are recorded by a conventional PDA, which is directly secured to the pile's surface. The PDA consists of a strain measurement device (type: TML FLA-2.350-11) and an accelerometer (type: Endevco 7270A) to measure the strain and acceleration in the axial direction, i.e. along the z-axis. Detailed information regarding the experimetnal setup, the properties and dimensions of the pile can be found in [6, 8].

The magnetic field components at the sensor location generated by the equivalent magnetic dipole are derived from the fundamental dipole field equation given by

$$\mathbf{B}_{\text{meas}}(\mathbf{r}) = \frac{\mu_0}{4\pi}\left[\frac{3\mathbf{r}(\mathbf{m}\cdot\mathbf{r})}{r^5} - \frac{\mathbf{m}}{r^3}\right]. \tag{4}$$

For a general distance $z(t)$ and for a relative vector $\mathbf{r} = \mathbf{r}_s - \mathbf{r}_d = (0, d, -z(t))$ and $\mathbf{m} = (0, 0, m_z)$, the dot product is $\mathbf{m}\cdot\mathbf{r} = -m_z z(t)$. Substituting these into the dipole field equation, the radial and axial field components are expressed as

$$B_{y,\text{meas}}(t) = G_y(d, z(t))\, m_z(t), \qquad B_{z,\text{meas}}(t) = G_z(d, z(t)\, m_z(t), \tag{5}$$

where the geometric transfer functions are

$$G_y(d, z(t)) = -\frac{\mu_0}{4\pi}\frac{3dz(t)}{(d^2 + z(t)^2)^{5/2}}, \qquad G_z(d, z(t)) = \frac{\mu_0}{4\pi}\frac{2z(t)^2 - d^2}{(d^2 + z(t)^2)^{5/2}}. \tag{6}$$

Before impact occurs ($t = 0$), the pile displacement is $z_p(t) = 0$, resulting in the initial vertical distance $z(0) = z_0$. The measured initial magnetic field components, $B_{y0,\text{meas}}$ and $B_{z0,\text{meas}}$, are then expressed as

$$B_{y0,\text{meas}} = G_y(d, z_0)\, m_0, \qquad B_{z0,\text{meas}} = G_z(d, z_0)\, m_0. \tag{7}$$

To determine the initial position, the ratio $R_0 = B_{y0,\text{meas}}/B_{z0,\text{meas}}$ is calculated, which elimi-

This work is licensed under CCBY 4.0

Media and Publishing Partner

nates the unknown m_0, resulting in

$$R_0 = \frac{-3dz_0}{2z_0^2 - d^2}. \tag{8}$$

Rearranging this expression yields the quadratic equation shown below

$$2R_0 z_0^2 + 3dz_0 - R_0 d^2 = 0. \tag{9}$$

Solving for the positive root provides the initial vertical distance z_0. Once z_0 is established, the pre-impact dipole moment is found as

$$m_0 = \frac{B_{y0,\text{meas}}}{G_y(d, z_0)}. \tag{10}$$

1.2 Dynamic Tracking of the Magnetic Center

The second phase of the analysis involves the calculation of the dynamic state parameters, $(m_{\text{dyn}}, z_{\text{dyn}})$, which characterize the dipole behavior during a hammer blow. As the impact-induced stress wave propagates through the steel monopile, the magnetic field is altered, causing the effective magnetic center to deviate from its pre-impact static position. In contrast to the static initialization described in the previous section, the system is now treated as a time-varying model driven by the instantaneous magnetic field ratio $R(t) = B_{y,\text{meas}}(t)/B_{z,\text{meas}}(t)$. The apparent position $z_{\text{dyn}}(t)$ is obtained by solving the quadratic geometry equation

$$2R(t)z_{\text{dyn}}(t)^2 + 3dz_{\text{dyn}}(t) - R(t)d^2 = 0 \tag{11}$$

at each sampled time step. Once the $z_{\text{dyn}}(t)$ position is obtained by taking the positive root of the above expression, the dynamic magnetisation $m_{\text{dyn}}(t)$ is calculated as

$$m_{\text{dyn}}(t) = \frac{B_{y,\text{meas}}(t)}{G_y(d, z_{\text{dyn}}(t))}. \tag{12}$$

The calculation of $z_{\text{dyn}}(t)$ and $m_{\text{dyn}}(t)$ yields two parameters resulting from the impact-induced stress. The first, the apparent spatial shift, $\Delta z(t)$, quantifies the offset of the magnetic centroid from the actual physical penetration depth

$$\Delta z(t) = z_{\text{dyn}}(t) - (z_0 + z_p(t)). \tag{13}$$

The second, the magnetisation change, $\Delta m(t)$, captures the change in dipole magnitude relative to the pre-impact state

$$\Delta m(t) = m_{\text{dyn}}(t) - m_0. \tag{14}$$

1.3 Magnetic Field Signal Decomposition

To isolate the specific drivers of the magnetic signal change during the impact, the total measured field $\mathbf{B}_{\text{meas}}$ is decomposed into three distinct components:

$$\mathbf{B}_{\text{meas}} = \mathbf{B}_{\text{geo}} + \mathbf{B}_{\Delta m} + \mathbf{B}_{\Delta z}, \tag{15}$$

This work is licensed under CCBY 4.0

Media and Publishing Partner NDTnet

in which $\mathbf{B}_{\text{geo}}$ represents the influence of pile displacement, $\mathbf{B}_{\Delta m}$ is the field due to the change in magnetisation, and $\mathbf{B}_{\Delta z}$ denotes the influence of the spatial shift. This separation allows for a decoupled analysis of the pile displacement versus the magnetic effects induced by the hammer blow. The first component related to the pile displacement represents the field that would be observed if the monopile acted as a permanent magnet with a constant moment m_0 moving with $z_{\text{phys}}(t) = z_0 + z_p(t)$, calculated as

$$\mathbf{B}_{\text{geo}}(m_0, z_{\text{phys}}) = \mathbf{G}(d, z_{\text{phys}})m_0. \tag{16}$$

The dynamic response to the impact is then categorized into two terms representing the magneto-mechanical interaction. The magnetisation influence, $\mathbf{B}_{\Delta m}$, accounts for the change in the magnitude of the magnetic moment due to stress-induced changes. This component is calculated assuming the magnetic source remains at the physical penetration depth as shown below

$$\mathbf{B}_{\Delta m}(m_{\text{dyn}} - m_0, z_{\text{phys}}) = \mathbf{G}(d, z_{\text{phys}})(m_{\text{dyn}} - m_0). \tag{17}$$

Conversely, the spatial shift influence, $\mathbf{B}_{\Delta z}$, represents the field fluctuations caused by the transient displacement of the magnetic centroid z_{dyn} relative to the physical position z_{phys}. This contribution is mathematically formulated as

$$\mathbf{B}_{\Delta z}(m_{\text{dyn}}, z_{\text{dyn}} - z_{\text{phys}}) = \left[\mathbf{G}(d, z_{\text{dyn}}) - \mathbf{G}(d, z_{\text{phys}})\right] m_{\text{dyn}} \tag{18}$$

Ultimately, the total measured magnetic field is expressed as the summation of these three constituent parts as

$$\mathbf{B}_{\text{meas}} = \mathbf{B}_{\text{geo}}(m_0, z_{\text{phys}}) + \mathbf{B}_{\Delta m}(m_{\text{dyn}} - m_0, z_{\text{phys}}) + \mathbf{B}_{\Delta z}(m_{\text{dyn}}, z_{\text{dyn}} - z_{\text{phys}}). \tag{19}$$

2. Results

During the experimental series, the sensor was positioned at seven distinct orientations around the pile, all at the same height from the ground. Magnetic North was established as the 0° reference point, with subsequent orientations spaced at 45° intervals. The 45° position itself was omitted from the study due to physical site constraints. At each test location, a minimum of 130 hammer impacts were recorded, with impact energies ranging from 75 kJ to 280 kJ. To facilitate a comparative analysis of these impacts both within and between orientations, the peak values of each time series are extracted. In addition to these peak values, the mean peak value per orientation and the time series of a representable hammer blow are also considered and compared.

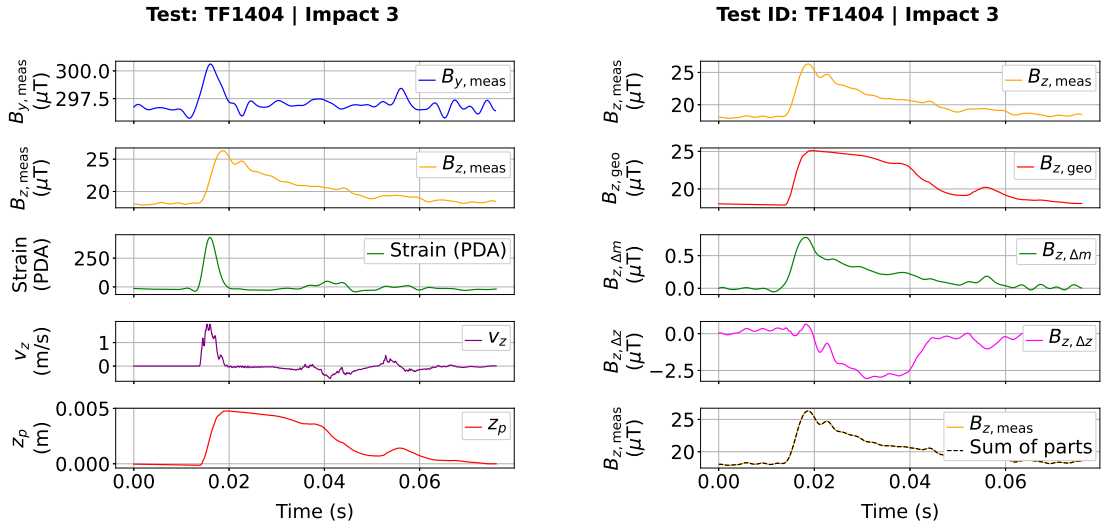
Fig. 2(a) shows the measured magnetic field signals in the radial ($B_{y,\text{meas}}$) and axial ($B_{z,\text{meas}}$) directions, presented in the first and second subplots, respectively, for impact 3 at the 0° orientation. The third subplot displays the axial strain signal for the same impact, as measured by the PDA. The strain signal exhibits a different magnitude and a narrower profile compared to the magnetic signals. The final two subplots show the pile velocity and displacement, which are derived by integrating the acceleration data. The resulting displacement, $z_p(t)$, is used to decompose the measured signal into its constituent components, as defined in Eq. 19.

Fig. 2(b) illustrates the decomposition of the axial magnetic field, $B_{z,\text{meas}}$, into its components, $B_{z,\text{geo}}$, $B_{z,\Delta m}$, and $B_{z,\Delta z}$, displayed in the second, third, and fourth subplots, respectively. The final subplot demonstrates that the summation of these components successfully reconstructs the total measured signal. As shown in the third subplot, the $B_{\Delta m}$ component, which accounts for stress-induced change in the magnetic field, has a lower peak magnitude and a different profile compared to the total magnetic signal. The same

This work is licensed under CCBY 4.0

Media and Publishing Partner

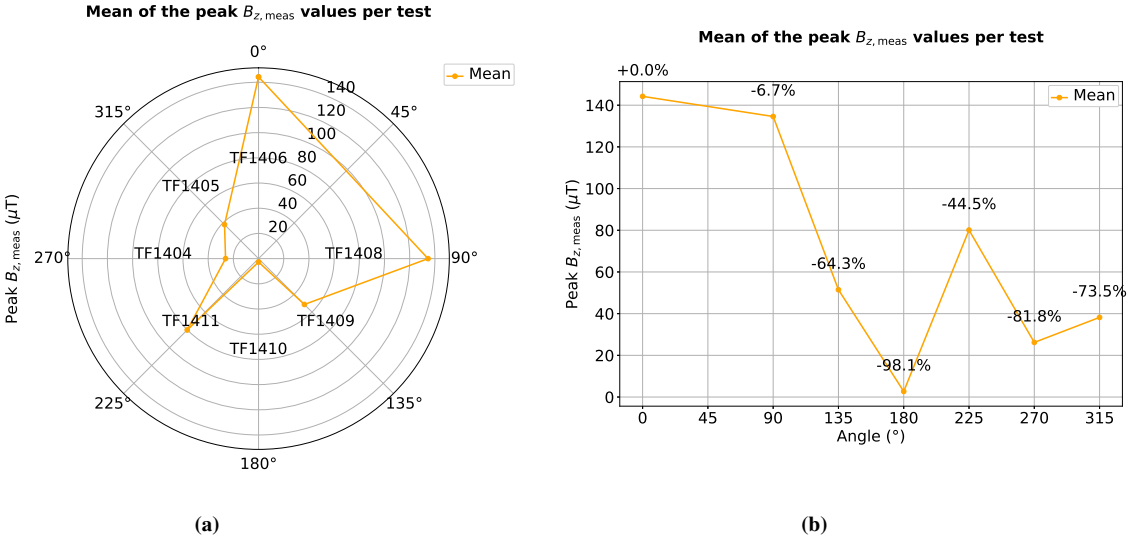
decomposition procedure can be applied to the radial magnetic field signal as well.



(a) (b)

Fig. 2. *(a) Measured signals for impact 3 at the 0° orientation; (b) Decomposition of the magnetic signal into its components as per Eq. 19.*

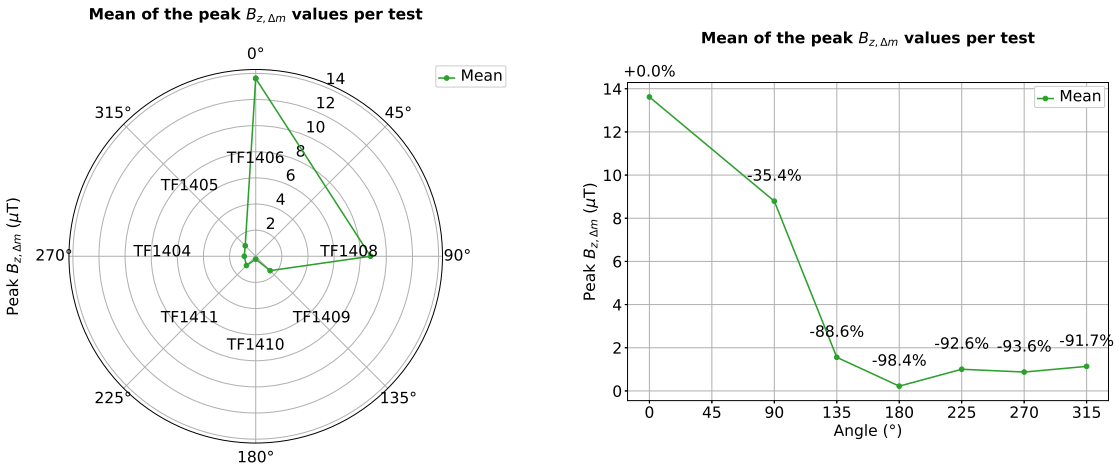
Strain measurements obtained from the PDA demonstrate consistent values for a given hammer energy across all positions around the pile. For a reliable and repeatable conversion from magnetic signals to strain, it is expected that the magnetic response remains uniform for a constant impact energy, regardless of sensor orientation. To evaluate this consistency, Fig. 3 presents the mean peak values of $B_{z,\text{meas}}$ for each test orientation, displayed in both polar (Fig. 3(a)) and cartesian (Fig. 3(b)) formats. As illustrated in these plots, the measured mean peak values vary between orientations. The relative percentage change with respect to the 0° chosen as the reference orientation is quantified in Fig. 3(b). The most significant deviation occurs at the 180° orientation, which exhibits a 98.1% difference from the baseline, followed by the 270° orientation with an 81.8% deviation. It should be noted that the behavior of the magnetic field at the 180° position is affected by the sensor's alignment with a longitudinal weld in the pile. The properties of the weld, which differ from those of the pile, significantly influence the magnetic field measurements at this location.



(a) (b)

Fig. 3. *Comparison of mean peak values for the total $B_{z,meas}$ signal across all sensor orientations: (a) Polar plot; (b) Cartesian plot displaying the percentage change in peak values relative to the 0° reference location.*

Fig. 4 presents a comparative analysis similar to the previous case, however, it focuses on the $B_{\Delta m}$ component derived from the decomposition process rather than the total measured magnetic signal. This component isolates the magnetic field changes induced by stress. As illustrated in both Fig. 4(a) and Fig. 4(b), the mean peak values for $B_{\Delta m}$ demonstrate notably improved consistency across the various sensor positions. This improvement is particularly evident within the range of the 135° and 315° orientations. This increased uniformity suggests that the decomposition successfully mitigates the influence of the pile's displacement which affects the total measured magnetic signal. Despite this improved consistency in the decomposed signal, high deviations relative to the other test locations persist at 0° and 90° orientations.



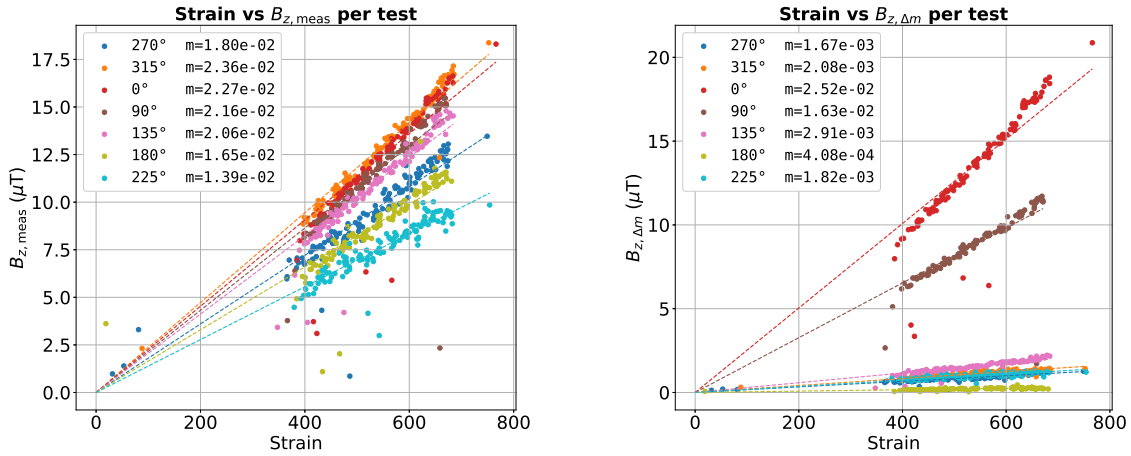
(a) **(b)**

Fig. 4. *Comparison of mean peak values for the decomposed stress-induced component ($B_{\Delta m}$) across all sensor orientations: (a) Polar plot and (b) Cartesian plot showing the improved consistency.*

While Fig. 3 and Fig.4 compare mean peak values where hundreds of impacts per orientation are averaged into a single data point, Fig. 5 evaluates whether the consistency of the $B_{\Delta m}$ component holds for individual impacts as well. To demonstrate that this improvement is not a results of averaging, Fig. 5 shows a comparison between the PDA-measured strain and the magnetic signal for every impact across all orientations. Specifically, Fig. 5(a) correlates the peak strain with the peak value of the total axial magnetic field ($B_{z,\text{meas}}$) for each impact. The resulting trendlines exhibit significant variations in their slopes, indicating a non-uniform relationship across the different sensor orientations. In contrast, Fig. 5(b) shows the same correlation but now using the decomposed $B_{\Delta m}$ component. In this case, the trendlines show to be closer to each other, particularly within the 135° to 315° range. Consistent with above-mentioned findings, the 0° and 90° orientations continue to display pronounced deviations from this general trend. This suggests that by decoupling the stress-induced magnetic change from the total measured signal, a more repeatable correlation between the magnetic field and strain measurements is achieved for individual impacts across various sensor positions. The discrepancies observed at the 0° and 90° orientations could be attributable to other interference sources or material inhomogeneities, which remain a subject for further investigation.

3. Conclusions

In this study, the influence of pile displacement on magnetic field measurements during pile driving was investigated. Using a magnetic dipole model, a signal decomposition method was implemented to separate the total measured signal into its stress-induced and pile displacement



(a) **(b)**

Fig. 5. *Correlation between measured axial strain and magnetic field peak values for individual impacts at each orientation: (a) Results using the total measured signal ($B_{z,meas}$), showing diverging trendlines; (b) Results using the stress-induced component ($B_{\Delta m}$).*

related components. The findings demonstrate that by isolating the stress-induced term, $B_{\Delta m}$, the influence of the pile's displacement was successfully mitigated. While the total measured signal $B_{z,\text{meas}}$ exhibited significant variance, the $B_{\Delta m}$ component showed a high consistency in peak values for individual impacts across different sensor orientations. This consistency, particularly evident within the 135° to 315° orientations range, confirms that removing the pile displacement related contributions yields to a repeatable relationship between the magnetic field measurements and the axial strain. Although deviations at 0° and 90° need further investigation, these results further validate the feasibility of using magnetic sensors as a reliable, non-contact method for strain monitoring in pile driving applications.

References

[1] WindEurope. Wind energy in europe: 2025 statistics and the outlook for 2026–2030. Technical report, WindEurope, Brussels, Belgium, February 2026.

[2] J. Chung, R. Wallerand, and M. Hélias-Brault. Pile fatigue assessment during driving. *Procedia Engineering*, 66:451–463, 2013.

[3] R. M. Buckley, R. J. Jardine, S. Kontoe, P. Barbosa, and F. C. Schroeder. Full-scale observations of dynamic and static axial responses of offshore piles driven in chalk and tills. *Géotechnique*, 70(8):657–681, 2020.

[4] E. Wisotzki, R. van Foeken, P. van Esch, and D. Novakovic. Strain and acceleration measurements at instrumentation distances to the pile head of 0.5 and 1.0 times the diameter—offshore pile-monitoring experience. In P. Bullock, G. Verbeek, S. Paikowsky, and D. Tara, editors, *10th International Conference on Stress Wave Theory and Testing Methods for Deep Foundations*, pages 506–519, West Conshohocken, PA, 2019. ASTM International.

[5] P. Wang, X. Tian, T. Peng, and Y. Luo. A review of the state-of-the-art developments in the field monitoring of offshore structures. *Ocean Engineering*, 147:148–164, 2018.

[6] P. C. Meijers, A. Tsouvalas, and A. V. Metrikine. Magnetomechanical response of a steel monopile during impact pile driving. *Engineering Structures*, 240:112340, 2021.

This work is licensed under CCBY 4.0

Media and Publishing Partner

[7] P. C. Meijers. *Non-collocated methods to infer deformation in steel structures: The magnetomechanical effect in cylindrical structures subjected to impact loads*. PhD thesis, Delft University of Technology, Delft, Netherlands, 2021.

[8] P. C. Meijers and F. Greco. Non-contact energy flux measurement of impact pile driving. In Á. Cunha and E. Caetano, editors, *Experimental Vibration Analysis for Civil Engineering Structures (EVACES 2025)*, volume 674 of *Lecture Notes in Civil Engineering*, pages 1–12. Springer, Cham, Switzerland, 2025.

This work is licensed under CCBY 4.0

Media and Publishing Partner